

Article

Source and Tectonic Setting of Porphyry Mo Deposits in Shulan, Jilin Province, China

Nan Ju ^{1,*}, Sen Zhang ¹, Lin-Lin Kou ¹, Hai-Po Wang ², Di Zhang ¹, Yu-Chao Gu ¹ and Tong Wu ¹

¹ Shenyang Center, China Geological Survey, Huanghe Street 280, Shenyang 110034, China; zhangsen556@163.com (S.Z.); koulinlin@126.com (L.-L.K.); zhangdi9521@163.com (D.Z.); guyi1224@126.com (Y.-C.G.); jesnet1981@163.com (T.W.)

² The sixth geological and mineral exploration institute of Inner Mongolia, Hulunbeier 021000, China; zltdr@126.com

* Correspondence: junan_cgs@163.com; Tel.: +86-18104025767

Received: 26 September 2019; Accepted: 24 October 2019; Published: 26 October 2019



Abstract: The Shulan area in Jilin Province is a part of the Lesser Xing'an–Zhangguangcai Range polymetallic ore belt, which is an important Cu–Mo ore region of northeast China. The discovery of three large Mo ore deposits (Fu'anbu, Chang'anbu, and Jidetun) highlights its potential for porphyry Mo ore deposits. Here we investigated the tectonic setting and mineralization of Mo ore deposits in the Shulan area, based on comparative study of the Fu'anbu, Chang'anbu, and Jidetun deposits. The ore-controlling structures are NE–SW- and NW–SE-trending faults. The main ore mineral in all three deposits is molybdenite. The ore bodies are all hosted in granites, have a stratiform or lenticular shape, and have strongly altered wall rocks. These observations indicate the Mo deposits in the Shulan area are typical porphyry Mo deposits. All were formed during the early Yanshanian (199.6–133.9 Ma). Biotite adamellites from the Chang'anbu deposit yield a U–Pb age of 182.10 ± 1.20 Ma. Molybdenites from the Fu'anbu and Jidetun deposits have Re–Os isochron ages of 166.9 ± 6.7 and 169.1 ± 1.8 Ma, respectively. Quartz and ore minerals were analysed for H–O and S–Pb isotopes, respectively. The results suggest the ore-forming materials were predominantly of upper-mantle origin, with secondary contributions from the lower crust. The ore-hosting granites have high concentrations of SiO₂ (66.67–75.43 wt.%) and Al₂O₃ (12.91–16.44 wt.%), low concentrations of MgO (0.09–1.54 wt.%), and Ritman index ($\sigma = K_2O + Na_2O)^2 / (SiO_2 - 43)$) ratios of 2.09–2.57. The granites are enriched in large-ion lithophile elements and depleted in high-field-strength elements, and have negative Eu anomalies. The ore-hosting rocks are geochemically similar to granites in northeastern China that were generated in a collisional orogeny. We conclude that early Yanshanian (199.6–133.9 Ma) mantle–crust-derived magmatism caused by the subduction of the Palaeo-Pacific Plate was the main source of Mo deposits in the Shulan area.

Keywords: porphyry Mo; geochemistry; S–Pb–H–O isotopes; ore genesis; Jilin Province; Shulan

1. Introduction

The Shulan area in Jilin Province is a part of the Lesser Xing'an–Zhangguangcai Range polymetallic ore belt. More than 10 large porphyry Mo deposits have been discovered in this belt, such as the Daheishan, Dashihe, Huojihe, and Lumin ore deposits. Recent discoveries have included the Jidetun Mo, Fu'anbu Mo, and Chang'anbu Cu–Mo deposits in the Shulan area, all of which are Mo deposits of medium scale. Further study of the Mo deposits in the Shulan area is important for future exploration in this region [1–6].

Molybdenum deposits in the Shulan area have similar features and comparable mineralization types, and are ideal for a comparative study. The ore bodies are mostly stratiform or lenticular, hosted in granitic rocks, and have strong wall-rock alteration. Their distribution is controlled by faults.

However, there is little information available regarding the geological setting, ore deposit geology, mineralization types, and exploration of Mo deposits in the Shulan area. As such, the formation mechanisms of Mo mineralization in this area are unclear.

The ore-forming materials of the deposits may be homologous with hydrothermal deposits, S–Pb and H–O isotopic compositions. In this paper, we describe the ore deposit geology and present S–Pb isotopic data for sulphides, H–O isotopic data for quartz–sulphide veins, and geochemical data for host rocks. These data are used to identify the fluids and metal sources involved in mineralization and the origins and tectonic setting of Mo mineralization in the Shulan area.

2. Geological Setting

The Shulan area lies on the northern margin of the North China Craton, between the deep-seated Yitong–Yilan and Dunhua–Mishan faults and at the intersection of the Xilamulun–Changchun and Yitong–Yilan faults. Tectonism in this area has been favorable for ore formation. The main strata in this area comprise Quaternary conglomerates, the Palaeogene Shulan Group (consisting of black or off-white sandstone and grey black mudstone), the Palaeogene Quliu Group (dominated by celadon-grey sandstone interbedded with shale and sandy shale), and the Permian Yangjiagou Group (comprising metamorphosed sandstone and slate). Multiple stages of magmatism occurred in the Hercynian (386–257 Ma), Indo-Chinese (257–205 Ma), and Yanshanian periods (199.6–133.9 Ma). Hercynian igneous rocks are dominated by plagioclase granites, biotite granites, and quartz diorites, whereas Indo-Chinese period igneous rocks are adamellites and granodiorites. Yanshanian igneous rocks are biotite adamellites, alkali feldspar granites, fine-grained granites, and granitic porphyry. The NW–SE-trending Xin’an–Emu Fault and NE–SW-trending Huoshidingzi–Chang’anbu Fault dominate the tectonic framework of the Shulan area. The migration and concentration of ore-forming elements were facilitated by these faults (Figure 1).

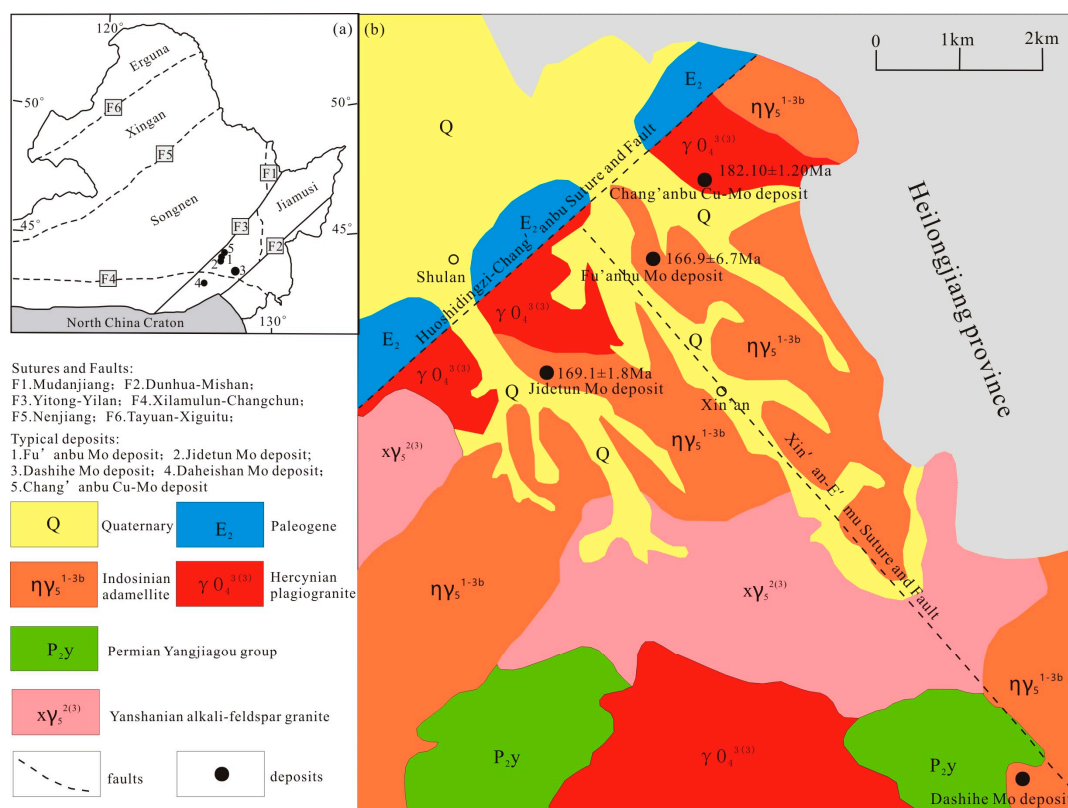


Figure 1. (a) Simplified tectonic map of the Shulan area and (b) geological map of the Shulan area (modified after [7]).

3. Ore Deposit Geology

3.1. Chang'anbu Mo Deposit

The intrusive rocks in the Chang'anbu Mo deposit are early Yanshanian quartz diorites, diorites–granodiorites, adamellites–syenogranites, and alkali feldspar granites–alkali granites [7]. These are calc-alkaline rocks with mixed crust and mantle sources. Pegmatite dykes and quartz veins are common. Evidence of faulting and other tectonic structures, such as fracture and gouge zones, slickenlines, and breccias is also widespread. The F1 fault is the primary fault in which the ore bodies are hosted (Figure 1), which is located to the south of the ore deposit and is E–W-trending. It is clear that the mineralization was controlled by tectonic structures. Chloritization, epidotization, kaolinization, sericitization, pyrophyllitization, silicification, and K-feldspathization has strongly affected the wall rocks. There is no obvious zonation in the types of alteration. Chalcopyrite and molybdenite are mostly present in altered granites, and occasionally in quartz veinlets. In general, the mineralization is closely associated with K-feldspathization and silicification.

(1) Cu orebodies characteristics: More than 10 Cu ore bodies have been found in this region. The largest is 1000 m in length, 480 m in width, has a total thickness of 83.2 m, and an average Cu grade of 0.52 wt.%. This ore body is hosted in biotite adamellite, which has a thick quartz vein above and below the intrusion. All of the ore bodies are E–W-trending and the largest are lenticular bodies, although other ore bodies are vein-type. The ores are mostly veinlet–disseminated or disseminated. The main ore minerals are chalcopyrite and pyrite.

(2) Mo orebody characteristics: There are more than 20 Mo orebodies in the region. The main ore body is also hosted in biotite adamellite, has a length of 2000 m and width of 720 m. Its total thickness is 266.4 m, with an average Mo grade of 0.088 wt.%. These Mo ore bodies are also nearly E–W-trending. The primary ore body is an irregular body, and the boundary between the ore body and wall rocks is unclear. The ores exhibit flaky, cataclastic, and metasomatic textures and veinlet–disseminated structures. The main ore minerals are molybdenite and pyrite.

(3) The coexistence of Cu and Mo is notable, which is a distinctive feature of porphyry Cu–Mo deposits. A small number of Cu ore bodies are present in quartz veins that cut Mo ore bodies, suggesting the Cu ore bodies formed after the Mo ore bodies (Figures 2 and 3). The wall rocks of the coexisting Cu–Mo ore bodies are mainly strongly altered biotite adamellite and K-rich granite [8].

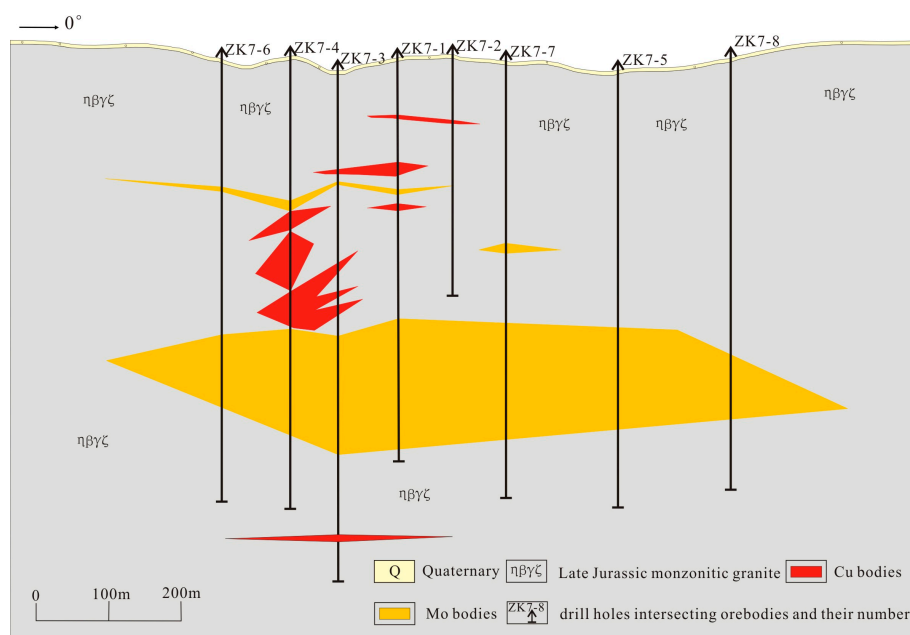


Figure 2. Geological cross-section of Line No. 7 through the Chang'anbu Cu–Mo ore deposit (modified after [8]).

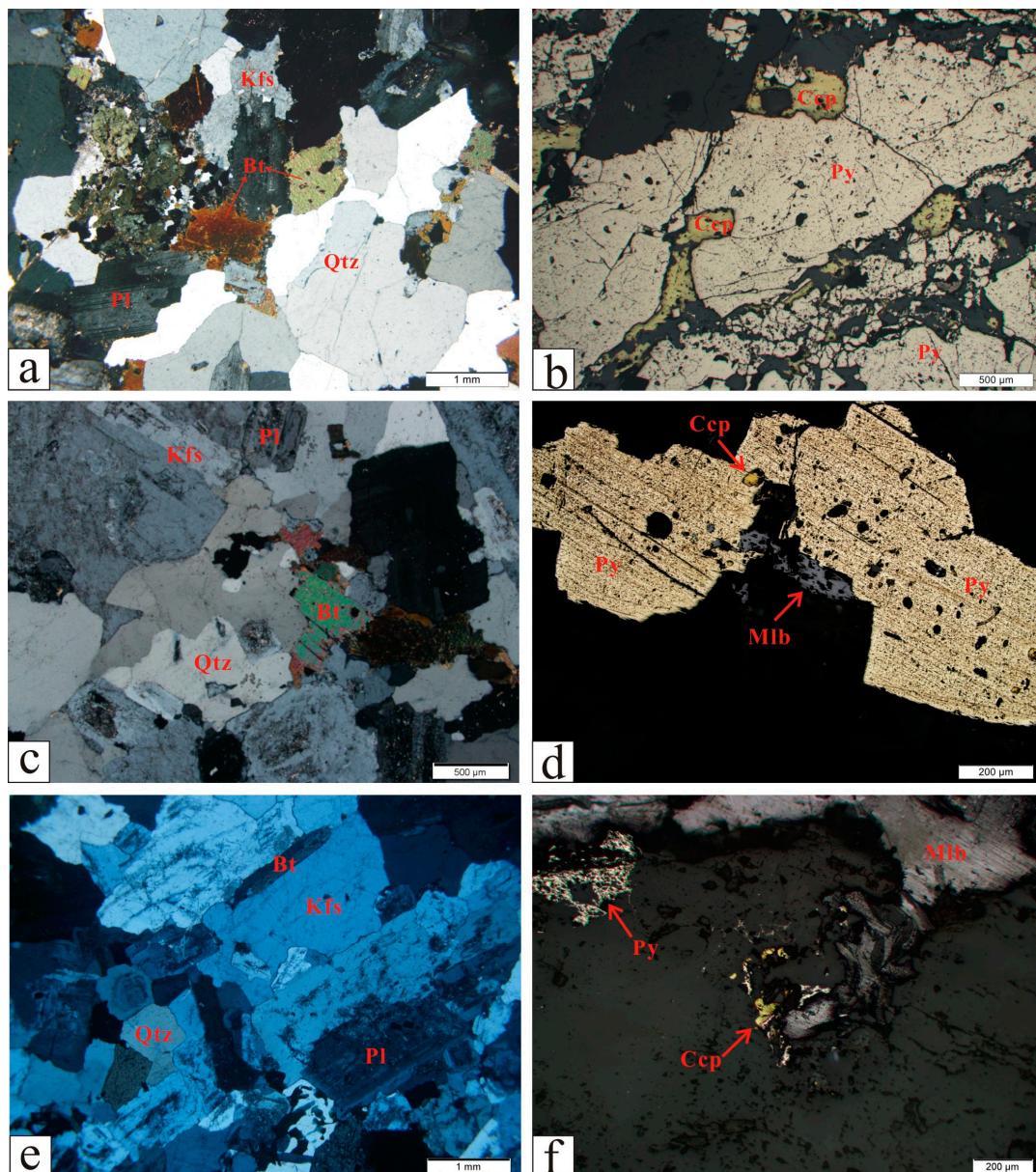


Figure 3. Photomicrographs of ore-hosting rock and microscopic mineralization characteristics of the Shulan Mo or Cu–Mo deposits: (a) adamellite and (b) chalcopyrite perforated pyrite from the Chang’anbu deposit; (c) granodiorite and (d) molybdenite perforated pyrite from the Fu’anbu deposit; (e) granodiorite and (f) molybdenite perforated chalcopyrite from the Jidetun deposit. Kfs = K-feldspar; Bt = biotite; Pl = plagioclase; Qtz = quartz; Ccp = chalcopyrite; Py = pyrite; Mlb = molybdenite).

3.2. Jidetun Mo Deposit

The Permian Yangjiagou Group crops out in the north of the Jidetun Mo deposit, which consists of black–grey slate, alternating metasandstones and metasiltstones, and local interbeds of tuffaceous sandstones and siltstones. Multi-stage faults are common in this region and are NW- and NE-trending. The ore deposit is controlled by a secondary NW-trending structure. Three magmatic events occurred in this region, represented by granodiorites, adamellites, and quartz monzonite intrusions, respectively. The first two intrusive events (i.e., granodiorites and adamellites) were most significant in ore deposit formation. Silicification, K-feldspathization, epidotization, kaolinization, and sericitization have affected the wall rocks. The alteration types overlap and exhibit no visible zonation.

Most ore bodies are hosted in granodiorites and adamellites. The largest ore body is 1300 m in length, 1200 m in width, and has an average Mo grade of 0.087 wt.%. Its thickness reaches 420 m in its central part and becomes thinner on the flanks. The ore body is horizontal with a stratiform shape, and branches at the flanks. The boundary between the ore body and wall rocks is not visible. The ores have scaly–flaky textures, stringer, stockwork and disseminated–vein, thin sheet, and disseminated–vein forms [9,10]. The main ore minerals are molybdenite and pyrite, whereas K-feldspar, plagioclase, quartz, and amphibole are the major gangue minerals (Figures 3 and 4).

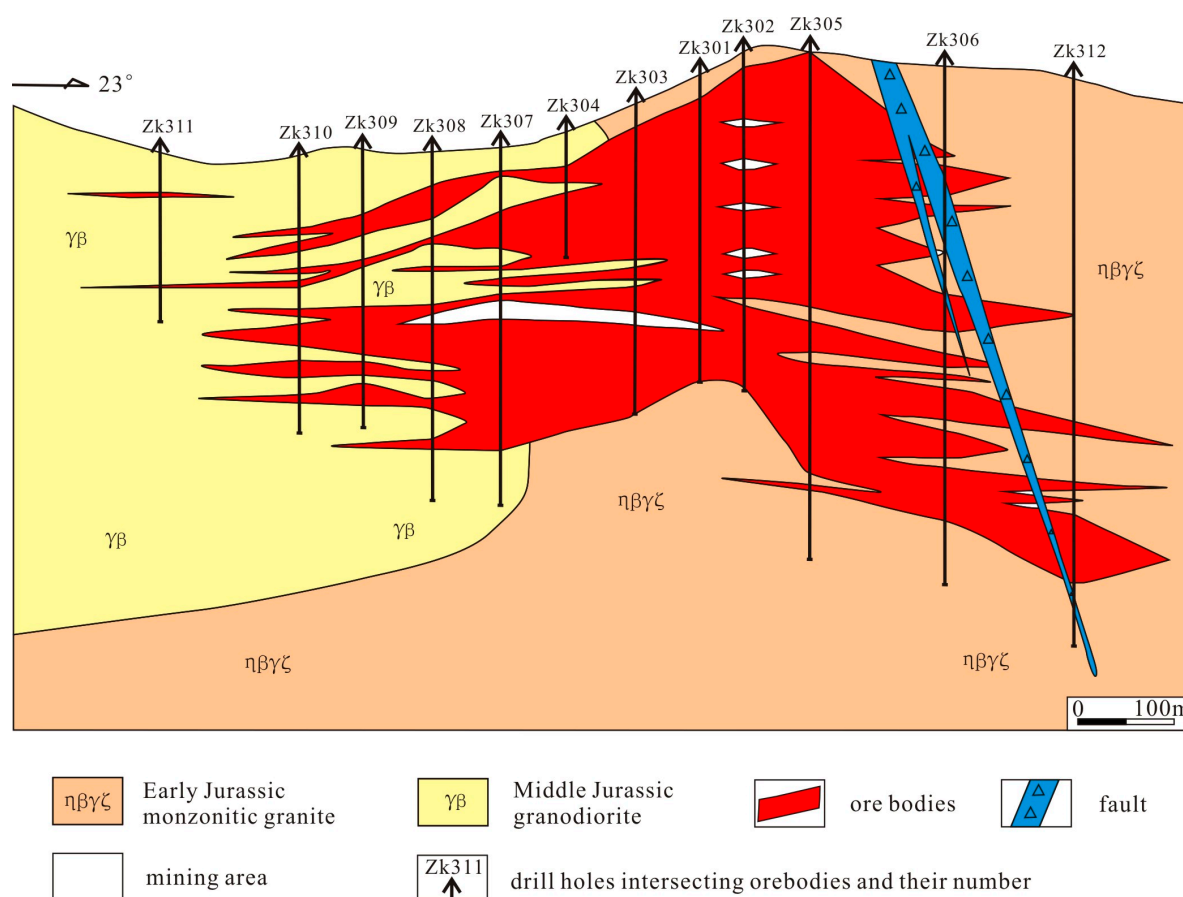


Figure 4. Geological cross-section of Line No. 3 through the Jidetun Mo ore deposit (modified after [9,10]).

3.3. Fu'anbu Mo Deposit

Quaternary rocks are exposed in the area of the Fu'anbu Mo deposit. Magmatism was extensive in this region, with Yanshanian magmatism being the most voluminous. Most of the Yanshanian igneous rocks are adamellites, along with some biotite granites and granitic porphyries, which are batholiths or dykes. The ore bodies were controlled by secondary faults, which are NW- and NE-trending. Zoning of alteration types is evident, reflecting a gradual transition from high–moderate–low temperatures. Silicification, K-feldspathization, sericitization, and muscovitization occurred in the inner zone of the orebodies, where mineralization was concentrated. Chloritization and kaolinization occurred in the outer zone.

A total of 10 Mo ore bodies have been discovered in this ore deposit. Ore Bodies No. I–IV extend in a northeastern direction, whereas Ore Bodies No. V–VII extend in an eastern direction. The No. X ore body extends in a northwestern direction (Figure 5). The largest ore body is the No. VIII ore body, which is 1300 m in length, with an average Mo grade of 0.133 wt.%. The ore body varies in thickness from 9 to 10 m, is thickest in its central part, has a vein-like or lenticular form, and strikes NW–SE

with a dip of 45–59°. The ore body bifurcates from SE to NW. The main ore mineral is molybdenite, along with small amounts of wolframite. Gangue minerals include K-feldspar, plagioclase, quartz, and biotite. The ores have anhedral–granular or metasomatic textures and disseminated–vein and stockwork forms [11].

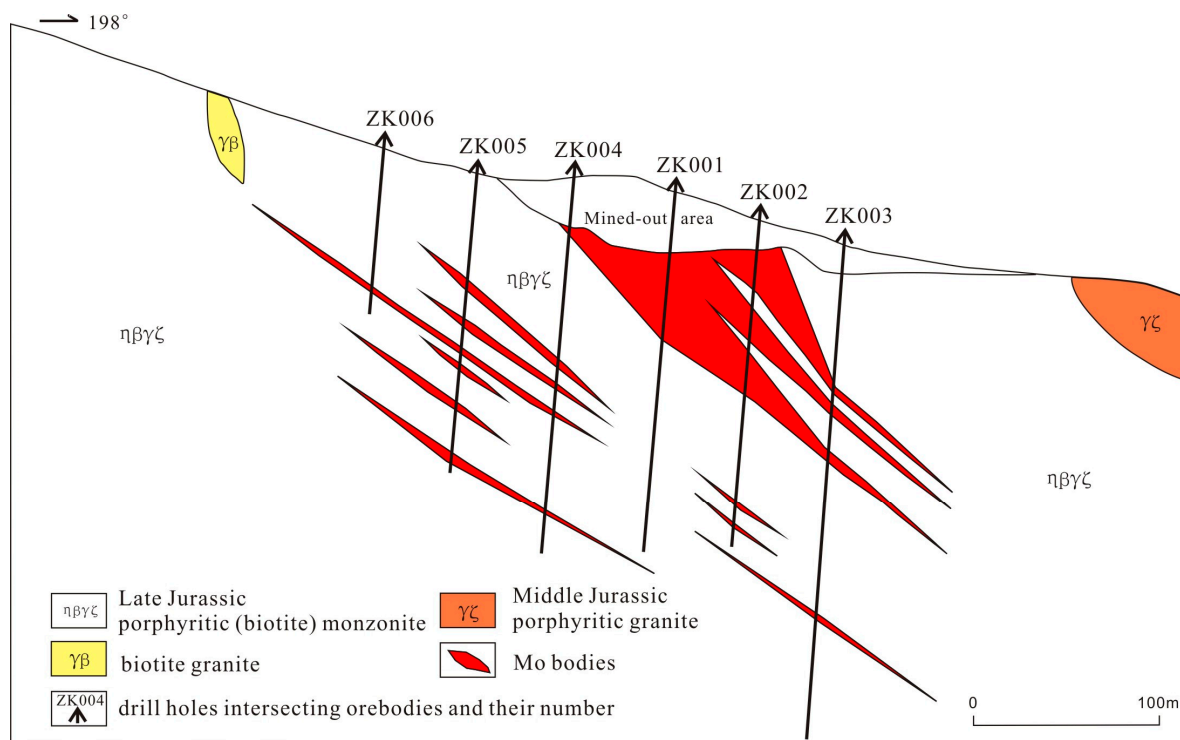


Figure 5. Geological cross-section of Line No. 0 through the Fu'anbu Mo ore deposit (modified after [11]).

3.4. Synthesis

A total of three studied medium–large Mo ore deposits (Chang'anbu, Jidetun, and Fu'anbu) have been discovered in the Shulan area. The ore deposit geology characteristics are listed in Table 1.

Two or three intrusive events have occurred in this region (166–182 Ma). The Mo or Cu–Mo ore bodies are mostly stratiform, nervate or lenticular, are hosted in granitic rocks, and have strong wall–rock alteration with some zonal characteristics (potash feldspathification–silicification). Their distribution is controlled by NE- and NW-trending faults. The ore mineral is dominantly molybdenite, along with some chalcopyrite, pyrite, pyrrhotite, and wolframite, with veinlet–disseminated characteristics.

Porphyry Mo deposits occur mostly in the interior of granite and surrounding rock masses. The shape of the ore body depends on the shape of the rock mass and includes layers, lenses, and veins. Therefore, ore deposits in the Shulan area have geological characteristics of typical porphyry Mo or Cu–Mo deposits [4,12].

Table 1. Geological characteristics of Mo deposits in the Shulan area (modified after [12]).

Deposits	Mineral	Ore-controlling Structure	Metallogenic Rock	Isotopic Age	Orebody Occurrence	Alteration of Wall Rock	Ore Minerals	References
Fu'anbu	Mo	NE-trending fault and NW-trending fault	adamellite	Molybdenites Re–Os isochron age of 166.9 ± 6.7 Ma	Split/within the rock mass	Potash feldspathization, sericitization, silicification, chloritization, epidotization	Molybdenite, pyrite	Modified after [10,12]
Jidetun	Mo	NE-trending fault and NW-trending fault	adamellite, quartz diorite	molybdenites Re–Os isochron age of 169.1 ± 1.8 Ma	Ellipsoid-like, stratiform-like/within the rock mass	Potash feldspathization, sericitization, silicification, epidotization, kaolinization, greisenization	Molybdenite, pyrite	Modified after [12]
Chang'anbu	Cu, Mo	Intersection of NE-trending fault and NW-trending fault, cryptoexplosive breccia pipe	biotite adamellite mainly	biotite adamellites U–Pb age of 182.10 ± 1.20 Ma	Stratiform, lenticular, veinlike/within the quartz vein and rock mass	Silicification, Potash feldspathization, carbonatation, chloritization, epidotization, argillization, sericitization	Molybdenite, pyrite, chalcopyrite, magnetite, sphalerite, galena	Modified after [12]

4. S–Pb–H–O Isotopes

4.1. Sample Preparation and Analytical Techniques

Twenty-nine samples, including 16 samples from the Chang'anbu deposit (Dc006, Dc007, and Dc008), 8 samples from the Fu'anbu deposit (Dxf115), and 5 samples from the Jidetun deposit (Dj118), were collected from drill cores. Sulphur and Pb isotopic analysis was conducted on sulphides from the ore samples, including molybdenite, pyrite, chalcopyrite, and pyrrhotite. Hydrogen and O isotopic analysis was conducted on quartz from quartz veins that contain molybdenite. The analyses were undertaken at the Laboratory of CNNC (China National Nuclear Corporation), Beijing Research Institute of Uranium Geology, China. Lead isotopes were determined with a IsoProbe thermal ionization mass spectrometer (TIMS). Sulphur isotopes were measured with a gas isotope ratio mass spectrometer (DeltaV Plus). Hydrogen and O isotopes were determined with a Flash EA elemental analyzer and a MAT253 gas isotope ratio mass spectrometer.

Pb isotope analysis: Powdered samples of 0.1–0.2 g were weighed and digested with mixed acid ($\text{HF} + \text{HNO}_3 + \text{HClO}_4$) in a low-pressure airtight digestion vessel (PFA). The aqueous solution was evaporated to dryness when it was fully dissolved after 24 h. The sample was again evaporated to dryness after reacting with HCl (6 mol/L) to form chloride. The sample was digested again with 1 mL HBr (0.5 mol/L) and separated through centrifugation. Further separation of clear liquid was performed on an anion exchange column (250 μL AG1 \times 8, 100–200 mesh) using HBr (0.5 mol/L) for elution. Dissociation of Pb was conducted with 1 mL HCl (6 mol/L). Pb was evaporated to dryness and kept in a PFA beaker for further analysis. Samples were stuck to a Re ribbon with phosphoric acid/silica gel and analyzed using an Isoprobe thermal ionisation mass spectrometer. Pb isotope ratios were measured using static receiving.

Sulphur isotope analysis: Monomineralic sulphide and cuprous oxide were ground to ~200 mesh and then evenly mixed. The mineral powders were subjected to a pressure of 2.0×10^{-2} Pa and temperature of 980 °C to make the gas of the sulphur dioxide. The gas was collected by frozen that is in the confined space. Sulphur isotope analysis was performed using a Delta V Plus gas isotope mass spectrometer. The analytical results are reported as $\delta^{34}\text{S}$ -V-CDT with an analytical precision better than $\pm 0.2\text{‰}$.

Hydrogen and oxygen isotope analyses: Quartz was ground to ~40–60 mesh and samples of 5–10 mg were weighed and heated in a thermostat drier at 105 °C for more than 4 h and then wrapped well with a clean and dry tin capsule for further measurements. Air in the elemental analyzer Flash EA was flushed and replaced by high-purity helium to reduce the background hydrogen. Samples were analyzed after the temperature reached 1400 °C and the background decreased to 50 mV. Quartz inclusions are decomposed in a ceramic tube containing carbon glass, resulting in the release of hydrogen gases such as H_2O and H_2 . The gases were reduced to H_2 as a result of the reaction with carbon at high temperature. High-purity helium was used as the carrier gas for H_2 . The analytical results are reported with respect to V-SMOW and analytical precision is better than $\pm 1\text{‰}$.

4.2. S–Pb Isotope Data

4.2.1. S Isotope Data

The $\delta^{34}\text{S}$ values of sulphides from the Chang'anbu deposit vary from 0.3‰ to 2.7‰, with an average of 1.3‰ (Table 2). Sulphides in ores from the Fu'anbu deposit have $\delta^{34}\text{S} = 2.8\text{--}4.0\text{‰}$, with an average of 3.4‰. $\delta^{34}\text{S}$ values of sulphides in ores from the Jidetun deposit range from 2.3‰ to 3.0‰, with an average of 2.6‰. The measured $\delta^{34}\text{S}$ values only show small variations, which is indicative of equilibrium S isotopic fractionation.

Table 2. S and Pb isotopic compositions of the Chang'anbu, Fu'anbu, and Jidetun ore deposits.

Deposit	Sample No.	Mineral	$\delta^{34}\text{S}$ (‰)	$\text{Pb}^{208}/\text{Pb}^{204}$	$\text{Pb}^{207}/\text{Pb}^{204}$	$\text{Pb}^{206}/\text{Pb}^{204}$
Fu'anbu	Dxf115-1-1	Pyrite	3.1	38.010	15.520	18.775
Fu'anbu	Dxf115-1-2	Molybdenite	3.6	37.970	15.508	18.261
Fu'anbu	Dxf115-2-1	Pyrite	3.0	37.983	15.515	18.280
Fu'anbu	Dxf115-2-2	Molybdenite	3.5	37.951	15.504	18.254
Fu'anbu	Dxf115-3-1	Pyrite	4.0	38.137	15.558	18.299
Fu'anbu	Dxf115-3-2	Molybdenite	3.7	37.935	15.497	18.283
Fu'anbu	Dxf115-4-1	Pyrite	2.8	38.079	15.624	18.167
Fu'anbu	Dxf115-4-2	Molybdenite	3.3	37.934	15.508	18.252
Jidetun	Dj118-1	Molybdenite	3.0	37.994	15.513	18.265
Jidetun	Dj118-2	Molybdenite	3.0	38.000	15.516	18.364
Jidetun	Dj118-3	Molybdenite	2.3	37.992	15.516	18.293
Jidetun	Dj118-4	Molybdenite	2.5	38.297	15.516	18.528
Jidetun	Dj118-5	Molybdenite	2.3	38.032	15.525	18.284
Chang'anbu	Dc006-1	Chalcopyrite	1.6	37.956	15.511	18.236
Chang'anbu	Dc006-2	Pyrite	2.7	38.079	15.541	18.267
Chang'anbu	Dc006-3	Pyrrhotite	1.9	37.956	15.514	18.290
Chang'anbu	Dc007-1	Chalcopyrite	1.6	37.942	15.504	18.221
Chang'anbu	Dc007-2	Pyrite	1.2	37.993	15.511	18.215
Chang'anbu	Dc007-3	Pyrrhotite	0.7	38.158	15.557	18.235
Chang'anbu	Dc008-1	Chalcopyrite	1.3	37.931	15.502	18.221
Chang'anbu	Dc008-2	Pyrite	1.5	37.999	15.551	18.046
Chang'anbu	Dc009-1	Pyrite	1.6	38.148	15.574	18.143
Chang'anbu	Dc009-2	Pyrrhotite	1.4	38.209	15.583	18.176
Chang'anbu	Dc0010-1	Pyrite	0.3	38.744	15.643	18.700
Chang'anbu	Dc0010-2	Pyrrhotite	0.5	38.819	15.655	18.734
Chang'anbu	Dc0011-1	Chalcopyrite	0.8	37.972	15.516	18.238
Chang'anbu	Dc0011-2	Pyrite	1.6	38.018	15.530	18.231
Chang'anbu	Dc0012	Molybdenite	1.6	38.081	15.538	18.300
Chang'anbu	Dc0013	Molybdenite	0.9	38.002	15.509	18.316

4.2.2. Pb Isotope Data

The $^{206}\text{Pb}/^{204}\text{Pb}$ ratios of sulphides in ores from the Chang'anbu deposit vary from 18.046–18.734, with small variations in $^{207}\text{Pb}/^{204}\text{Pb}$ (15.502–15.655) and $^{208}\text{Pb}/^{204}\text{Pb}$ ratios (37.931–38.819). The Fu'anbu deposit has $^{206}\text{Pb}/^{204}\text{Pb}$ ratios of 18.167–18.775, with small variations in $^{207}\text{Pb}/^{204}\text{Pb}$ (15.497–15.624) and $^{208}\text{Pb}/^{204}\text{Pb}$ (37.934–38.137) ratios. Sulphides in ores from the Jidetun deposit show little Pb isotopic variability, with $^{206}\text{Pb}/^{204}\text{Pb}$, $^{207}\text{Pb}/^{204}\text{Pb}$, and $^{208}\text{Pb}/^{204}\text{Pb}$ ratios of 18.265–18.528, 15.513–15.525, and 37.992–38.297, respectively.

4.3. H–O Isotope Data

The $\delta_{\text{V-SMOW}}$ values of quartz in the Chang'anbu deposit vary from -102.2‰ to -93.42‰ with an average of -97.9‰ (Table 3). $\delta^{18}\text{O}_{\text{V-SMOW}}$ values range from 9.1‰ to 11.6‰ , with an average of 10.2‰ . This compositional range is slightly larger than that of typical magmatic waters, and is indicative of fluid involvement from other possible sources. Quartz in the Fu'anbu deposit has $\delta_{\text{V-SMOW}}$ values between -79.5‰ and -96‰ , with an average of -91.8‰ . $\delta^{18}\text{O}_{\text{V-SMOW}}$ values vary from 8.5‰ – 9.8‰ , with an average of 9.0‰ . $\delta_{\text{V-SMOW}}$ (-99.2‰ to -108.2‰ ; average = -103.5‰) and $\delta^{18}\text{O}_{\text{V-SMOW}}$ (8.2‰ – 9.0‰ ; average = 8.8‰) values of quartz in the Jidetun deposit are similar to those of the Chang'anbu and Fu'anbu deposits. The compositional range is again slightly larger than that of typical magmatic water. Fluid inclusions in ore-bearing quartz veins yielded homogenization temperatures for the Chang'anbu, Fu'anbu, and Jidetun deposits of $273\text{--}380\text{ °C}$, $395\text{--}405\text{ °C}$, and $278\text{--}282\text{ °C}$, respectively (data are not publicly available). These represent the mineralization temperatures of the ore deposits (homogenization temperatures reflect minimal temperatures of the mineral deposition).

Table 3. H and O isotopic composition of quartz from molybdenite-quartz veins of the Chang'anbu, Fu'anbu and Jidetun ore deposits.

Deposit	Sample No.	Mineral	δD_{V-SMOW} (‰)	$\delta^{18}O_{V-SMOW}$ (‰)	$\delta^{18}O$ Water (‰)	Homogenization Temperature (°C)
Fu'anbu	OHf115-1	Quartz	−96.0	8.5	4.4	395.6
Fu'anbu	OHf115-2	Quartz	−79.5	9.8	5.7	401.2
Fu'anbu	OHf115-3	Quartz	−94.1	9.1	5.0	402.5
Fu'anbu	OHf115-4	Quartz	−93.9	8.6	4.5	398.2
Fu'anbu	OHf115-5	Quartz	−95.4	9.1	5.0	403.1
Jidetun	OHj003	Quartz	−108.2	8.2	0.5	279.2
Jidetun	OHj004	Quartz	−99.2	8.8	1.1	281.1
Jidetun	OHj005	Quartz	−102.6	9.0	1.3	278.4
Jidetun	OHj006	Quartz	−105.2	9.0	1.1	280.5
Jidetun	OHj007	Quartz	−102.2	9.0	1.3	279.0
Chang'anbu	OHc006	Quartz	−93.4	9.2	2.4	301.4
Chang'anbu	OHc007	Quartz	−96.4	9.1	1.8	288.9
Chang'anbu	OHc008	Quartz	−96.5	10.4	3.4	298.2
Chang'anbu	OHc009	Quartz	−100.4	11.6	5.0	308.7
Chang'anbu	OHc014	Quartz	−96.4	10.9	4.4	310.7
Chang'anbu	OHc015	Quartz	−102.2	10.2	3.4	302.6
Chang'anbu	OHc016	Quartz	−98.2	9.8	2.7	293.1
Chang'anbu	OHc017	Quartz	−99.3	10.7	3.4	289.0

5. Geochemistry of the Ore-Hosting Rocks

5.1. Sample Preparation and Analytical Techniques

A total of nine samples of ore-hosting rocks were collected from drill cores, among which sample Hxc001-003 is from the Chang'anbu deposit, sample Hxf001-004 is from the Fu'anbu deposit, and sample Hxj001-002 is from the Jidetun deposit. Mineralization and alteration are not evident in these samples of the ore-hosting rocks. Major element data were obtained by X-ray fluorescence spectrometry on an AB-104L PW2404 instrument. Trace elements were analyzed by inductively coupled plasma-mass spectrometry (ICP-MS) on an Elan DCR-e type instrument. After the removal of altered surfaces, fresh whole-rock samples were crushed to 200 meshes in an agate mill. Loss on ignition was determined by placing 100 mg of sample in a furnace at 980 °C for several hours, cooling the sample in a desiccator and then reweighing the sample. The rock reference materials AGV-2 (USGS) and GSR-3 (National Geological Standard Reference Materials of China) were used to monitor analytic accuracy and precision. Precision and accuracy are better than 5% for major elements and 10% for trace elements shown from repeated analyses. All major and trace element analyses were carried out at the Laboratory of CNNC, Beijing Research Institute of Uranium Geology, China [13]. The major and trace element data are listed in Tables 4 and 5, respectively.

Table 4. Major element data for ore-hosting rocks from the Chang'anbu, Fu'anbu, and Jidetun ore deposits (wt.%).

Deposit	Sample No.	SiO ₂	Al ₂ O ₃	TFe ₂ O ₃	MgO	CaO	Na ₂ O	K ₂ O	MnO	TiO ₂	P ₂ O ₅	FeO	LOI
Chang'anbu	Hxc001	52.91	16.44	17.65	0.157	1.36	3.90	6.94	0.14	0.20	0.06	4.94	0.14
Chang'anbu	Hxc002	68.89	15.00	3.14	1.05	2.78	3.65	3.97	0.07	0.42	0.12	1.73	0.89
Chang'anbu	Hxc003	66.67	15.12	4.08	1.54	3.46	3.68	3.40	0.08	0.53	0.16	2.07	1.24
Fu'anbu	Hxf001	69.89	15.48	2.38	0.54	2.01	4.44	3.76	0.03	0.35	0.13	0.52	0.95
Fu'anbu	Hxf002	72.92	13.91	2.16	0.41	1.60	3.97	3.94	0.05	0.21	0.06	1.05	0.77
Fu'anbu	Hxf003	71.41	15.06	1.97	0.35	1.44	4.35	4.19	0.04	0.31	0.10	0.75	0.77
Fu'anbu	Hxf004	70.45	15.25	2.40	0.57	1.89	4.56	3.73	0.04	0.39	0.13	1.04	0.57
Jidetun	Hxj001	74.17	13.38	1.69	0.16	0.95	3.04	5.82	0.03	0.11	0.03	0.8	0.62
Jidetun	Hxj002	75.43	12.91	1.24	0.09	0.72	3.43	5.34	0.02	0.09	0.02	0.58	0.67

Table 5. Trace element data for ore-hosting rocks from the Chang'anbu, Fu'anbu, and Jidetun ore deposits (ppm).

Deposit	Sample No.	Li	Be	Sc	V	Cr	Co	Ni	Cu	Zn	Ga	Rb	Sr	Y	Mo	Cd	In
Chang'anbu	Hxc001	13.7	2.27	2.67	34.30	21.20	6.26	1.46	21.60	99.60	28.30	214	196	9.46	1.21	0.07	0.05
Chang'anbu	Hxc002	14.1	2.51	5.32	51.70	175	6.08	4.59	18.10	58.30	18.30	110	300	18.50	4.73	0.07	0.03
Chang'anbu	Hxc003	18.9	1.75	6.82	62.50	44.40	8.75	3.69	16.70	58.90	16.20	86.9	397	13.30	20.20	0.08	0.04
Fu'anbu	Hxf001	36.6	2.74	3.15	27.40	44.40	3.41	2.19	4.63	57.90	23.70	106	492	6.74	1.01	0.03	0.03
Fu'anbu	Hxf002	50.1	4.02	2.72	18.50	55.90	2.98	2.15	5.20	42.40	19.00	163	176	20.10	1.12	0.05	0.02
Fu'anbu	Hxf003	11.6	2.69	2.42	22.40	92	2.46	3.06	5.18	47.90	20.60	97.7	421	8.24	1.68	0.09	0.02
Fu'anbu	Hxf004	30.8	2.89	3.13	31.90	129	3.62	3.86	5.61	60.80	22.30	101	486	7.98	2.46	0.04	0.03
Jidetun	Hxj001	14.3	1.22	1.12	10.40	135	1.29	2.54	13.90	25.40	15.90	84.5	82.9	3.73	3.27	0.21	0.01
Jidetun	Hxj002	8.67	1.71	0.84	7.01	38.50	0.69	1.00	35.40	19.40	16.30	115	43.3	5.03	0.85	0.32	0.01
Deposit	Sample No.	Sb	Cs	Ba	La	Ce	Pr	Nd	Sm	Eu	Gd	Tb	Dy	Ho	Er	Tm	Yb
Chang'anbu	Hxc001	0.27	7.52	505	13.70	22.60	2.23	9.29	1.5	0.47	1.39	0.25	1.39	0.28	0.86	0.15	1.16
Chang'anbu	Hxc002	0.31	8.58	435	25.70	48.10	5.51	20.30	3.78	0.84	3.17	0.59	3.09	0.61	1.88	0.33	2.45
Chang'anbu	Hxc003	0.53	6.18	442	18.20	34.80	4.26	17.30	3.26	0.81	2.72	0.46	2.47	0.48	1.37	0.23	1.56
Fu'anbu	Hxf001	0.11	2.50	770	20.90	39.80	5.05	19.70	3.16	0.77	2.37	0.33	1.45	0.23	0.60	0.09	0.64
Fu'anbu	Hxf002	0.17	9.85	349	23.20	56.20	5.14	18.80	3.65	0.61	3.27	0.60	3.37	0.69	2.04	0.38	2.75
Fu'anbu	Hxf003	0.14	1.78	724	27.20	52.80	5.66	21.00	3.3	0.71	2.66	0.36	1.64	0.28	0.76	0.12	0.79
Fu'anbu	Hxf004	0.16	2.31	698	26.10	52.50	6.26	23.70	4	0.88	2.9	0.40	1.77	0.27	0.74	0.11	0.74
Jidetun	Hxj001	0.09	2.7	314	15.10	45.60	3.10	10.90	1.65	0.38	1.51	0.18	0.803	0.14	0.40	0.06	0.46
Jidetun	Hxj002	0.25	2.42	214	12.00	23.50	2.48	8.59	1.43	0.26	1.21	0.19	0.92	0.17	0.51	0.09	0.61
Deposit	Sample No.	Lu	W	Re	Tl	Pb	Bi	Th	U								
Chang'anbu	Hxc001	0.17	1.45	0.01	1.17	33.40	0.23	15.20	2.34								
Chang'anbu	Hxc002	0.37	6.43	0.01	0.79	22.20	0.10	34.10	8.09								
Chang'anbu	Hxc003	0.23	1.86	0.01	0.64	20.00	0.09	14.40	5.22								
Fu'anbu	Hxf001	0.09	1.50	<0.01	0.69	20.80	0.05	7.97	0.91								
Fu'anbu	Hxf002	0.40	2.06	<0.01	0.99	23.70	0.04	25.30	2.87								
Fu'anbu	Hxf003	0.10	3.10	0.01	0.55	18.00	0.03	7.78	1.27								
Fu'anbu	Hxf004	0.10	4.11	<0.01	0.58	20.60	0.09	9.27	1.57								
Jidetun	Hxj001	0.07	4.46	<0.01	0.46	25.60	0.03	16.80	1.39								
Jidetun	Hxj002	0.10	1.44	0.01	0.67	21.80	0.04	10.50	1.14								

5.2. Major Element Data

In the Chang'anbu deposit, three biotite adamellite samples have high concentrations of SiO₂ (66.67–68.89 wt.%) and Al₂O₃ (15.00–16.44 wt.%), and low concentrations of TiO₂ (0.2–0.53 wt.%) and P₂O₅ (0.06–0.16 wt.%). The sample with SiO₂ = 52.91 wt.% is mineralized. These samples are slightly K-rich (K₂O/Na₂O = 0.92–1.78) and have relatively high total alkali contents (K₂O + Na₂O = 7.08–10.84 wt.%). The σ ($\sigma = [\text{K}_2\text{O} + \text{Na}_2\text{O}]^2 / [\text{SiO}_2 - 43]$) ratios vary from 2.12 to 2.24, indicative of the calc-alkaline series ($\sigma < 3.3$).

In the Jidetun deposit, two granite samples are characterized by high concentrations of SiO₂ (74.17–75.43 wt.%) and Al₂O₃ (12.91–13.38 wt.%), and low concentrations of TiO₂ (0.09–0.11 wt.%) and P₂O₅ (0.02–0.03 wt.%). These samples have relatively high total alkali contents (K₂O + Na₂O = 8.77–8.86 wt.%) and are K-rich (K₂O/Na₂O = 1.56–1.91). The σ ratios of 2.37–2.52 are indicative of the calc-alkaline series.

In the Fu'anbu deposit, four adamellite samples have high concentrations of SiO₂ (69.89–72.92 wt.%) and Al₂O₃ (13.91–15.48 wt.%), and low TiO₂ (0.21–0.39 wt.%) and P₂O₅ (0.06–0.13 wt.%) contents. These samples have relatively high total alkali contents (K₂O + Na₂O = 7.91–8.54 wt.%) and are Na-rich (K₂O/Na₂O = 0.82–0.99). The σ ratios of 2.09–2.57 classify these samples as being calc-alkaline.

In a total alkalis–silica (TAS) classification diagram (Figure 6b), data for samples from the Chang'anbu deposit plot in the granodiorite field, while samples from the Jidetun and Fu'anbu deposits plot in the granite field. In general, all samples belong to the sub-alkaline series. In an F-M-A rock series discrimination diagram (Figure 6c), the samples are classified as being calc-alkaline. Figure 6a,d shows that all samples belong to the high-K and tholeiitic series. In an A/NK (Al₂O₃/[Na₂O + K₂O]) versus A/CNK (Al₂O₃/[CaO + Na₂O + K₂O]) discrimination diagram (Figure 6e), data for all samples plot in the metaluminous field. In summary, the ore-hosting rocks of the Chang'anbu, Jidetun, and Fu'anbu

deposits are metaluminous and calc-alkaline, with similar major element characteristics. However, samples from the Chang’anbu and Jidetun deposits have relatively higher concentrations of K, whereas samples from the Fu’anbu deposit have higher Na.

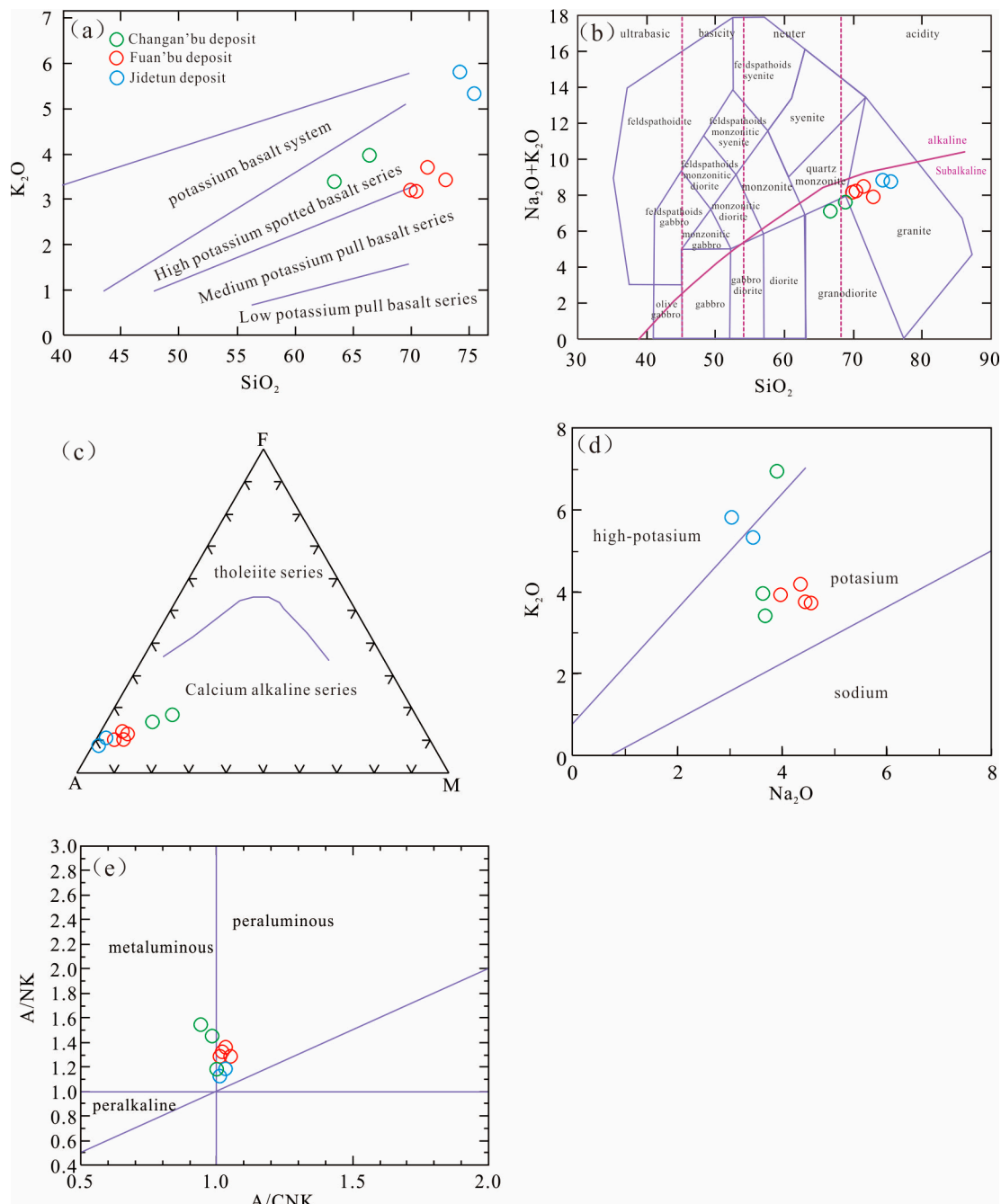


Figure 6. Major element diagrams for ore-hosting rocks from the Chang’anbu, Fu’anbu, and Jidetun deposits [13]. (a) SiO₂ – K₂O; (b) SiO₂ – K₂O + Na₂O; (c) F–A–M; (d) Na₂O – K₂O; (e) A/CNK–A/NK.

5.3. Trace Element Data

Ore-host rocks from the Chang’anbu, Fu’anbu, and Jidetun deposits have similar trace element features (Table 5). They are characterized by positive large-ion lithophile element (LILE; e.g., Rb) and negative high-field-strength element (HFSE; e.g., Ti) anomalies, which are indicative of a possible enriched mantle source. In primitive-mantle-normalized, multi-element diagrams (Figure 7a), the samples have patterns similar to granites, indicating a relatively deep origin. Thorium and

Pb also show significant enrichments, and Sr is depleted with primitive mantle. These characteristics are similar to those of rocks that form in subduction zones [14–20].

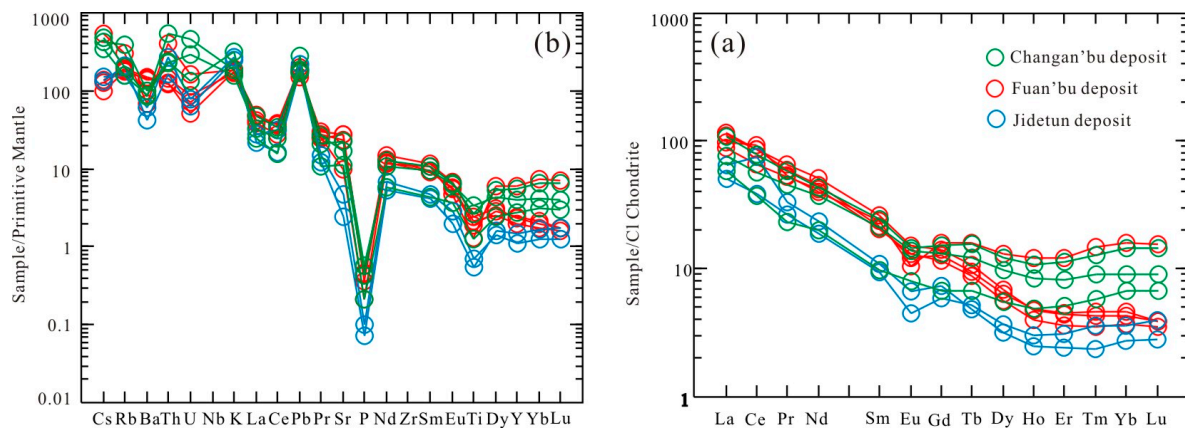


Figure 7. Primitive-mantle-normalized multi-element and chondrite-normalized rare earth element (REE) patterns for ore-hosting rocks from the Chang'anbu, Fu'anbu, and Jidetun deposits. (a) primitive-mantle-normalized multi-element patterns for ore-hosting rocks; (b) chondrite-normalized rare earth element (REE) patterns for ore-hosting rocks.

Ore-hosting rocks from the Chang'anbu, Fu'anbu, and Jidetun deposits have similar rare earth element (REE) patterns that are heavy REE (HREE)-depleted and light REE (LREE)-enriched ($LREE/HREE = 7.93\text{--}21.11$). The fractionation between the LREE and HREE also indicates a relatively deep origin. Total REE concentrations are relatively low, with large variations between 0.06 and 56.2 ppm. The samples also have relatively high $(La/Yb)_N$ (8.44–32.86) and $(Rb/La)_N$ (3.59–15.62) ratios, and large negative Eu anomalies ($\delta Eu = 0.18\text{--}0.33$). Negative Eu and Sr anomalies are mostly caused by plagioclase fractionation. Given that Eu^{3+} has a similar ionic radius to Ca^{2+} , it can replace Ca^{2+} in carbonate minerals (calcite vein), leading to negative Eu anomalies in granites. Therefore, we conclude that there was plagioclase fractionation or alteration in granitic rocks of the Jidetun deposit. Figure 7b shows the HREE-depleted nature of the samples, which indicates garnet was a residual phase in the magma source [21–25]. This requires the involvement of magmas from the deep crust or mantle.

6. Discussion

6.1. Ore-Forming Sources

Hydrogen and O isotopes ore-forming fluids, whereas S–Pb isotopes can reveal the nature of ore-forming sources. Previous studies of porphyry deposits in the Lesser Xing'an–Zhangguangcai Range ore belt have acquired a considerable amount of S–Pb–H–O isotopic data. $\delta^{34}S$ values of sulphides from the Daheishan Mo deposit vary from 0.4–3.0‰, whereas $\delta^{34}S$ values of sulphides from the Fu'anbu Mo deposit range from 1.5‰ to 4.1‰ [26]. This indicates multiple sources for the ore-hosting rocks and ores (i.e., mixed sources). Most of the ore deposits have Pb isotopic compositions are similar to those of subduction zone magmatism, indicating the ore-hosting rocks and ore-forming materials were derived from the crust and mantle. In summary, S–Pb isotopic data indicate that the ore-forming materials of the porphyry Cu–Mo deposits in the Lesser Xing'an–Zhangguangcai Range ore belt were derived from the deep mantle, but with some involvement of crustal material [27–34].

Quartz of the Fu'anbu deposit has $\delta D = -79.5\text{‰}$ to -96‰ and $\delta^{18}O_{H_2O} = 4.44\text{--}5.74\text{‰}$. Data for all samples plot in the field of primary mantle and magmatic waters (Figure 8d), implying that the ore-forming fluids were dominated by mantle and magma sources, but closer to the magmatic–water field, with slight involvement of meteoric water. $\delta^{34}S$ values of molybdenite (average = 3.2‰) from the ores are heavier than those of pyrite (average = 3.5‰). This indicates equilibrium fractionation of S isotopes between molybdenite and pyrite, which thus precipitated in the same physical and chemical

system. In general, the $\delta^{34}\text{S}$ variations are small (2.8–4.0‰), and broadly consistent with those of the mantle, magmas (0‰ \pm 3‰), and meteorites (0‰ \pm 3‰) [12,26]. The $\delta^{34}\text{S}$ values also overlap those of granites. These features suggest that the S in the ores was derived from deeply sourced magma [35] (Figure 8c). Pb isotopic compositions of most samples from the Fu'anbu deposit have a narrow range of values, indicating common origins or evolutionary process. Most ores plot between the evolution curves for orogenic belts and mantle, indicating derivation from magmatic Pb during an orogenic event. However, data for individual ores plot across the evolution curves for upper crust and mantle, suggesting a mixed mantle and upper-crustal source of Pb, and indicating a more complex source for the Fu'anbu deposit (Figure 8a,b).

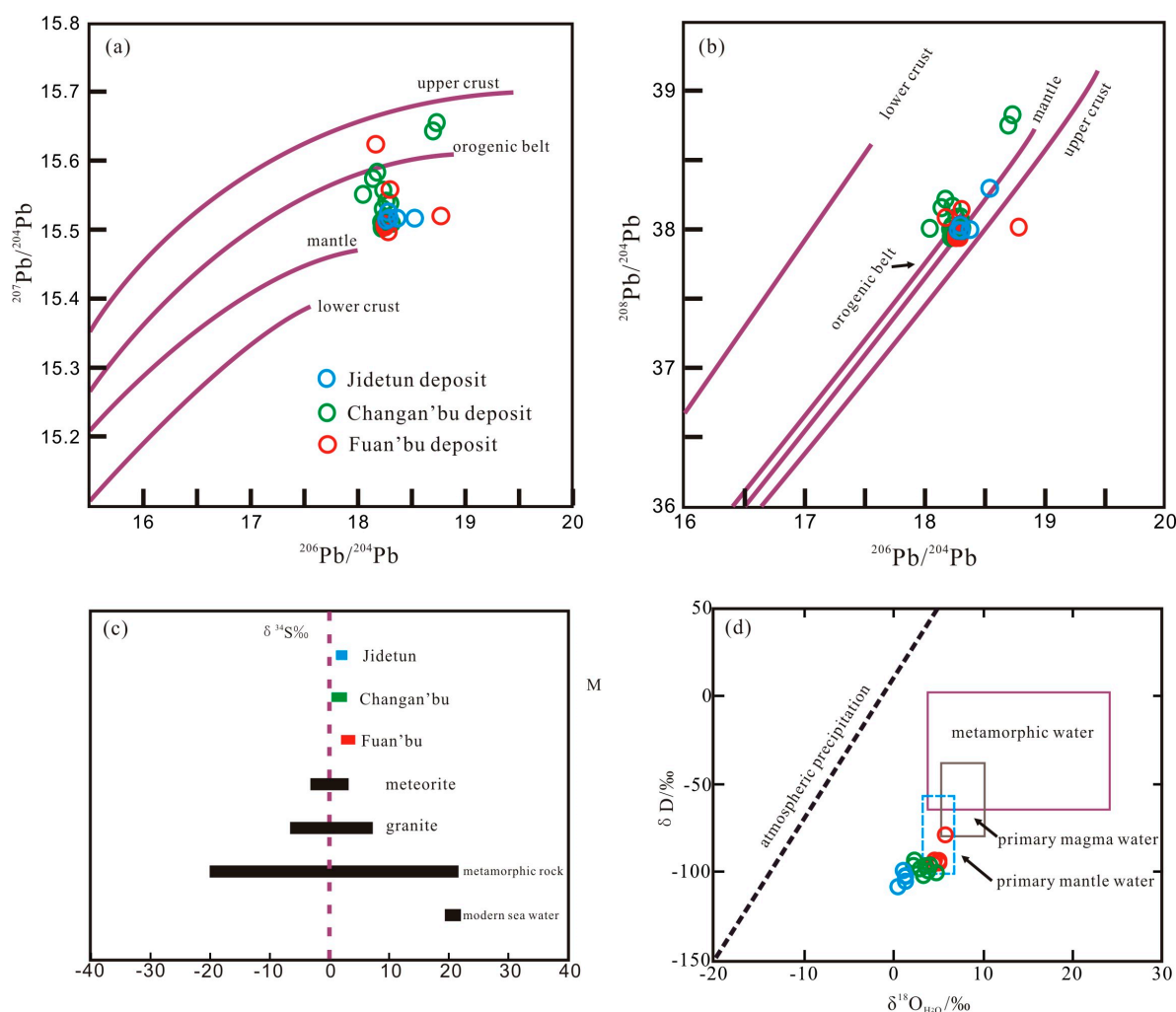


Figure 8. Pb and S source diagram for sulphides. δD versus $\delta^{18}\text{O}_{\text{H}_2\text{O}}$ discrimination diagram for fluids from the Chang'anbu, Fu'anbu, and Jidetun deposits [34–36]. (a) $^{206}\text{Pb}/^{204}\text{Pb}$ – $^{207}\text{Pb}/^{204}\text{Pb}$; (b) $^{206}\text{Pb}/^{204}\text{Pb}$ – $^{208}\text{Pb}/^{204}\text{Pb}$; (c) $\delta^{34}\text{S}$ content discrimination; (d) $\delta^{18}\text{O}_{\text{H}_2\text{O}}$ – δD .

Quartz in the Chang'anbu deposit has $\delta\text{D} = -102.2$ ‰ to -93.4 ‰ and $\delta^{18}\text{O}_{\text{H}_2\text{O}} = 9.1$ – 11.6 ‰. Data for all samples plot in the transitional field between magmatic and meteoric water, but closer to the magmatic water field (Figure 8d). The ore-forming fluids were derived from magmatic meteoric waters. Changes in the physical and chemical conditions of the magmatic waters were responsible for the precipitation of the ores. Average $\delta^{34}\text{S}$ values of chalcopyrite, pyrite, pyrrhotite, and molybdenite are similar and 1.3‰, 1.5‰, 1.1‰, and 1.3‰, respectively, indicative of a simple sulphur source. In general, the $\delta^{34}\text{S}$ values are broadly consistent with those of the mantle and magmas (0‰ \pm 3‰), and granites and meteorites. These features suggest the sulphur in the ores was derived from a deeply

sourced magma (Figure 8c). Apart from two samples (Dc010-1 and Dc010-2), Pb isotopic ratios of the four sulphide minerals are distributed on a line between the evolution curves for mantle and orogenic belts. The two exceptions plot in the field between orogenic belts and upper crust (Figure 8a,b). As such, Pb in the Chang'anbu deposit is a mixture of Pb from mantle-derived magma and radiogenic Pb from the country rocks. Minor Pb contributions from the upper crust are also evident.

Quartz in the Jidetun deposit has $\delta D = -108.2\text{‰}$ to -99.22‰ and $\delta^{18}O_{H_2O} = 8.2\text{--}9.0\text{‰}$. Data for all samples plot in the transitional field between magmatic and meteoric water (Figure 8d). The precipitation of the ores may have been due to the mixing of the two different fluids. The small $\delta^{34}S$ variations (2.3–3.0‰) of molybdenite from the Jidetun Mo deposit is evidence of a single origin (Figure 8c). These $\delta^{34}S$ values overlap those of the mantle, magmas, and meteorites, implying that the S in the molybdenite was derived from deeply sourced magma. Lead isotopic ratios of ores from the Jidetun deposit plot in the field between the mantle and orogenic belt curves, indicating the Pb was magmatically sourced from the deep mantle during an orogenic event (Figure 8a,b).

The S–Pb isotopic characteristics of the three deposits indicate that the ore-forming fluid of Mo or Cu–Mo deposits in the Shulan area could have arisen from the mixing of crustal and mantle materials, with their H–O isotopic signatures suggesting that the ore-forming fluids were derived from magmatic and meteoric waters. The Jidetun deposit had lower homogenisation temperatures and water $\delta^{18}O$ values, possibly because the ore-forming fluid of this deposit was derived from a single source and had not been superimposed by multiple hydrothermal processes. On the basis of this investigation of these three Mo and Mo–Cu deposits, we conclude that magmatism related to subduction contributed most ore-forming materials in the Shulan area. Near subduction zones, plates were subducted into the asthenosphere, where the crust was then heated, fused, and mixed with mantle material. There was thus higher contribution from the lower crust and upper mantle [34–36].

6.2. Tectonic Setting of Mineralisation

Geochronological data for the mineralization in the Shulan area and Lesser Xing'an–Zhangguangcai Range ore belt has been previously published. Biotite adamellites from the Chang'anbu deposit have a U–Pb age of 182.10 ± 1.20 Ma [8]. Molybdenites from the Fu'anbu and Jidetun deposits have Re–Os isochron ages of 166.9 ± 6.7 and 169.1 ± 1.8 Ma [36,37], respectively. Re–Os isochron ages of molybdenites from the Daheishan (168.2 ± 3.2 Ma) and Dashihe (186.7 ± 5.0 Ma) deposits [37–41], which are similar to the three deposits in the Shulan area, have also been reported. Combined with other geochronological data from northeastern China [12,42–46], three Mesozoic, large-scale, Mo ore-forming in the Shulan area have been identified, as follows.

(1) From 250–190 Ma, a collision between the North China and Palaeo-Asian plates occurred, which produced a high viscosity granitic magma derived mainly from the crust and is associated with the formation of Cu–Mo ore deposits.

(2) From 200 to 130 Ma, the Palaeo-Pacific Plate started to subduct beneath the Eurasian Plate, causing mixing of crust and mantle and forming a series of E–W- and NE–SW-trending faults, eventually leading to large mineralization events in the Shulan area.

(3) From 150–120 Ma, intermediate–silicic magmas and ore-forming fluids formed due to the collision between the North China and Siberian plates. As subduction of the Pacific Plate intensified, it became the circum-Pacific tectonic zone, with a new ore-forming system. Mineralization in northeast China represents several tectonic events, which involved multiple plates [8,12].

The ages of the ore-hosting rocks and ores in the Shulan area are consistent with those of regional Mo ore deposit formation, which was a large-scale, Jurassic, porphyry Mo mineralization event in northeastern China.

Ore-hosting rocks from the Chang'anbu, Fu'anbu, and Jidetun deposits have high SiO_2 and Al_2O_3 concentrations, low MgO concentrations, and σ ratios of 2.09–2.57. In addition, they are characterized by enrichment of LILE and LREE, depletion of HFSE, and negative Eu anomalies. These geochemical signatures are similar to those of granites in northeastern China that were generated in a collisional orogeny [8,30].

Granites can be classified into A-, S-, M-, and I-types. A-type granites are typically emplaced within rift zones or stable continental plates. In contrast, S-type granites are derived by partial melting of supracrustal or sedimentary source rocks. M-type granites are typically part of ophiolite suites and originate by fractionation of mafic magma. I-type granites are a suite of metaluminous, calc-alkaline granitic rocks. The I- and S-types are orogenic granites, but the A-type is not [12,35,39]. According to our study, the ore-hosting granitic rocks from the Mo deposits are I-type granites. In various tectonic setting or source discrimination diagrams (Figure 9), data for these granitic rocks plot in the field of I- and S-type granites. Moreover, the aluminous saturation index ($A/CNK = 0.92\text{--}1.05$) is less than 1.1. Together with the geochemical characteristics of northeastern China, these samples should thus be classified as I-type granites [12,43,47]. In general, they are orogenic granites derived from a crustal or mixed crust–mantle source. Slab-derived fluids also participate in the formation of orogenic granites. Thus, it is concluded that the porphyry Mo deposits in the Shulan area were formed in a orogenic setting associated with subduction.

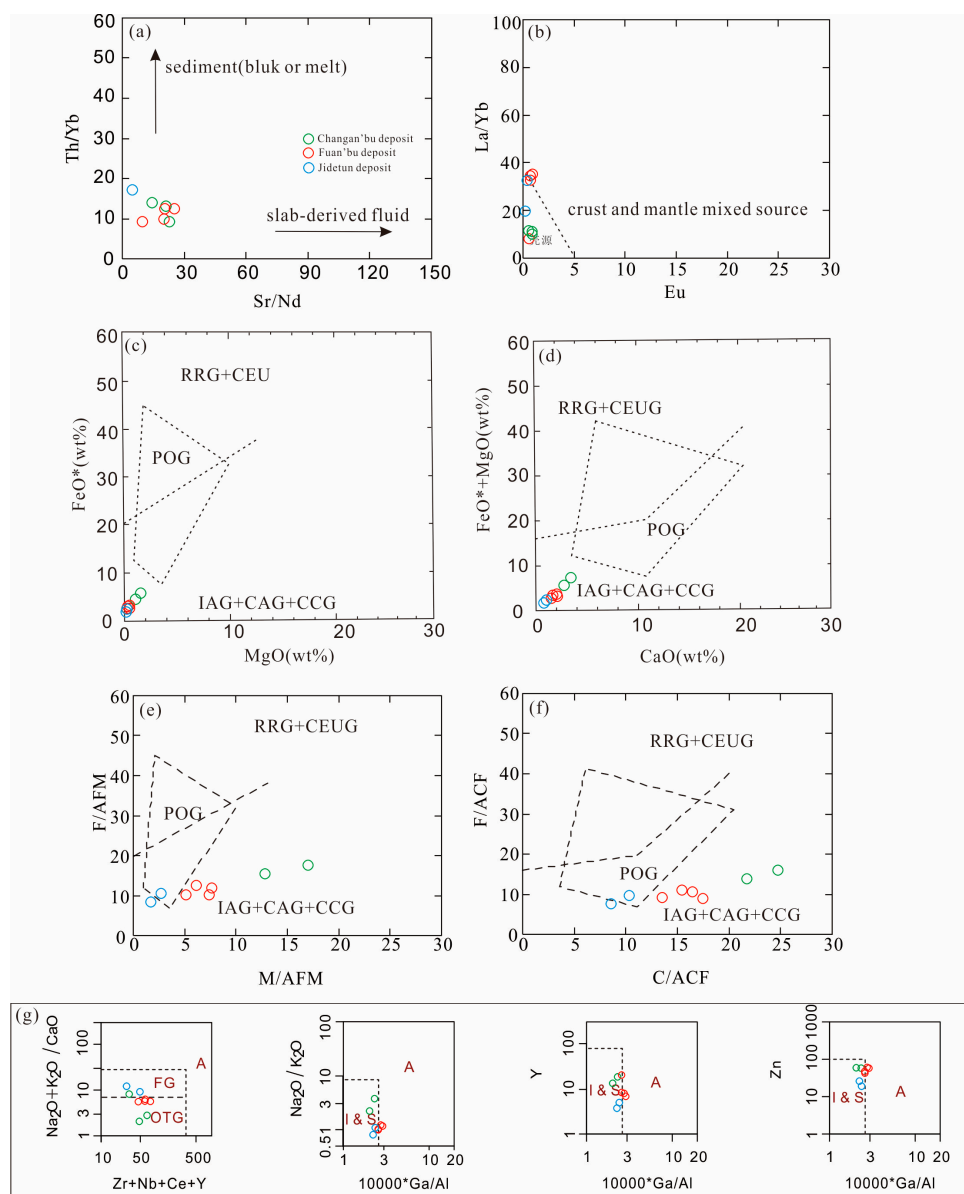


Figure 9. Tectonic setting and source discrimination diagrams for ore-hosting rocks from the Chang’anbu, Fu’anbu, and Jidetun deposits [5,6,13,30,35,36]. (a) Sr/Nd–Th/Yb; (b) Eu–La/Yb; (c) MgO–FeO; (d) CaO – FeO + MgO; (e) M/AFM–F/AFM; (f) C/ACF–F/ACF; (g) A–I–S type discrimination.

Large-scale, early Yanshanian magmatism (subducted oceanic) resulting from the melting of the lower crust and upper mantle was the most critical factor for the formation of the numerous porphyry Cu–Mo deposits in the Shulan area.

7. Conclusions

(1) Mo ore bodies in the Shulan area are mostly stratiform or lenticular, hosted in granitic rocks, and have strongly altered wall rocks. The ore body distribution is controlled by NE–SW- and NW–SE-trending faults. The ore mineral is dominantly molybdenite, along with some chalcopyrite, pyrite, and wolframite. The Mo deposits in the Shulan area are typical porphyry Mo or Cu–Mo deposits.

(2) Ore sources of the three Mo deposits in the Shulan area are dominated by magma generated by the subduction of the Palaeo-Pacific Plate. The ore-hosting rocks are geochemically similar to granites from northeastern China that were generated in a plate subducting.

(3) Early Yanshanian magmatism resulting from the melting of the lower crust and upper mantle was responsible for the widespread porphyry mineralization in the Shulan area.

Author Contributions: Conceptualization, S.Z.; Data curation, D.Z.; Methodology, Y.-C.G. and L.-L.K.; Software, H.-P.W. and T.W.; Writing—original draft and Writing—review & editing, N.J.

Funding: This research was funded by the National Key R&D Program of China, grant No. 2018YFC0604200.

Acknowledgments: We thank the assistance of Qingqing Shang and Xin-hao Sun from the College of Earth Science, Jilin University, Changchun, China.

Conflicts of Interest: The authors declare no conflict of interest.

References

- Zhang, L.C.; Wu, H.Y.; Wan, B. Ages and Geodynamic Settings of Xilamulun Mo–Cu Metallogenic Belt in the Northern Part of the North China Craton. *Gondwana Res.* **2009**, *16*, 243–254. [[CrossRef](#)]
- Deng, J.; Wang, Q.F.; Li, G.J.; Santosh, M. Cenozoic tectono-magmatic and metallogenic processes in the Sanjiang region, southwestern China. *Earth Sci. Rev.* **2014**, *138*, 268–299. [[CrossRef](#)]
- Yang, L.Q.; Deng, J.; Goldfarb, R.J.; Zhang, J.; Gao, B.F.; Wang, Z.L. 40Ar/39Ar geochronological constraints on the formation of the Dayingezhuang gold deposit: New implications for timing and duration of hydrothermal activity in the Jiaodong gold province, China. *Gondwana Res.* **2014**, *25*, 1469–1483. [[CrossRef](#)]
- Shu, Q.H.; Chang, Z.S.; Lai, Y.; Zhou, Y.T.; Sun, Y.; Yan, C. Regional metallogeny of Mo-bearing deposits in northeastern China, with new Re–Os dates of porphyry Mo deposits in the northern Xilamulun district. *Econ. Geol.* **2016**, *8*, 1783–1798. [[CrossRef](#)]
- Sengor, A.M.C.; Natal'in, B.A. *Paleotectonics of Asia: Fragments of Synthesis and the Tectonic Evolution of Asia*; Cambridge University Press: Cambridge, UK, 1996; pp. 486–640.
- Johnson, M.F.; Wang, C.Y.; Wang, P. Continental Island from the Upper Silurian (Ludfordian Stage) of Inner Mongolia: Implications for Eustasy and Paleogeography. *Geology* **2001**, *29*, 955–958. [[CrossRef](#)]
- Ju, N.; Ren, Y.-S.; Zhang, S.; Bi, Z.-W.; Shi, L.; Zhang, D.; Shang, Q.-Q.; Yang, Q.; Wang, Z.-G.; Gu, Y.-C.; et al. Metallogenic Epoch and Tectonic Setting of Saima Niobium Deposit in Fengcheng, Liaoning Province, NE China. *Minerals* **2019**, *9*, 80. [[CrossRef](#)]
- Ju, N.; Ren, Y.; Zhang, S.; Kou, L.; Zhang, D.; Gu, Y.; Yang, Q.; Wang, H.; Shi, L.; Sun, Q.; et al. The Early Jurassic Chang'anbu porphyry Cu–Mo deposit in Northeastern China: Constraints from zircon U–Pb geochronology and H–O–S–Pb stable isotopes. *Geol. J.* **2017**, *53*, 2437–2448. [[CrossRef](#)]
- Zeng, Q.D.; Liu, J.M.; Zhang, L.C. Re–Os Geochronology of Porphyry Molybdenum Deposit in South Segment of Da Hinggan Mountains, Northeastern China. *J. Earth Sci.* **2010**, *21*, 390–401. [[CrossRef](#)]
- Wu, G.; Chen, Y.J.; Zeng, Q.T. Zircon U–Pb Ages of the Metamorphic Supracrustal Rocks of the Xinghuadukou Group and Granitic Complexes in the Argun Massif of the Northern Great Hinggan Range, NE China, and Their Tectonic Implications. *J. Asian Earth Sci.* **2012**, *49*, 214–233. [[CrossRef](#)]
- Liu, W.Z. Study on the Geological Features and Genetic Type of the Fu'anbu Molybdenum Deposit, Jilin Province. Master's Thesis, Jilin University, Changchun, China, 2014. (In Chinese with English Abstract)

12. Chen, Y.J.; Zhang, C.; Li, N.; Yang, Y.F.; Deng, K. Geology of the Mo Deposits in Northeast China. *J. Jilin Univ. Earth Sci. Ed.* **2012**, *42*, 1223–1268. (In Chinese with English Abstract)
13. Khashgerel, B.-E. Geology and Reconnaissance Stable Isotope Study of the Oyu Tolgoi Porphyry Cu-Au System, South Gobi, Mongolia. *Econ. Geol.* **2006**, *101*, 503–522. [[CrossRef](#)]
14. Zeng, Q.D.; Liu, J.M.; Zhang, Z.L. Geology Fluid Inclusion and Sulfur Isotope Studies of the Chehugou Porphyry Molybdenum Copper Deposit, Xilamulun Metallogenic Belt, NE China. *Resour. Geol.* **2011**, *61*, 241–258. [[CrossRef](#)]
15. Drafting Group of Regional Stratigraphic Scale of Jilin Province. Stratigraphic scale of NE, China: Fascicule of Jilin Province. *Geol. Press* **1978**, *4*, 81–151. (In Chinese)
16. Mao, J.W.; Zhang, Z.C.; Zhang, Z.H. Re-Os Isotopic Dating of Molybdenites in the Xiaoliugou W (Mo) Deposit in the Northern Qilian Mountains and Its Geological Significance. *Geochim. Cosmochim. Acta* **1999**, *63*, 1815–1818.
17. Zeng, Q.D.; Liu, J.M.; Zhang, Z.L. Geology and Geochronology of the Xilamulun Molybdenum Metallogenic Belt in Eastern Inner Mongolia, China. *Int. J. Earth Sci.* **2011**, *100*, 1791–1809. [[CrossRef](#)]
18. Tang, H.S.; Chen, Y.J.; Santosh, M. REE Geochemistry of Carbonates from the Guanmenshan Formation Liaohe Group, NE Sino-Korean Craton: Implications for Seawater Compositional Change During the Great Oxidation Event. *Precambrian Res.* **2012**, *227*, 316–336. [[CrossRef](#)]
19. Qiu, K.F.; Deng, J.; Taylor, R.D.; Song, K.R.; Song, Y.H.; Li, Q.Z.; Goldfarb, R.J. Paleozoic magmatism and porphyry Cu-mineralization in an evolving tectonic setting in the North Qilian Orogenic Belt, NW China. *J. Asian Earth Sci.* **2016**, *122*, 20–40. [[CrossRef](#)]
20. Qiu, K.-F.; Taylor, R.D.; Song, Y.-H.; Yu, H.-C.; Song, K.-R.; Li, N. Geologic and geochemical insights into the formation of the Taiyangshan porphyry copper–molybdenum deposit, Western Qinling Orogenic Belt, China. *Gondwana Res.* **2016**, *35*, 40–58. [[CrossRef](#)]
21. Tang, H.S.; Chen, Y.J.; Wu, G. Paleoproterozoic Positive $\delta^{13}\text{C}$ Excursion in the Northeastern Sinokorean Craton: Evidence of the Lomagundi Event. *Gondwana Res.* **2011**, *19*, 471–481. [[CrossRef](#)]
22. Davis, G.A.; Zheng, Y.D.; Wang, Z. Mesozoic Tectonic Evolution of the Yanshan Fold and Thrust Belt, with Emphasis on Hebei and Liaoning Province, Northern China. *Colorado Geol. Soc. Am. Mem.* **2001**, *191*, 171–197.
23. Wan, B.; Hegner, E.; Zhang, L.C. Rb-Sr Geochronology of Chalcopyrite from the Chehugou Porphyry Mo–Cu Deposit (Northeast China) and Geochemical Constraints on the Origin of Hosting Grantechnology. *Econ. Geol.* **2009**, *104*, 351–363. [[CrossRef](#)]
24. Zorin, Y.A.; Zorina, L.; Spiridonov, A.M. Geodynamic Setting of Gold Deposits in Eastern and Central trans-bnikal (Chita Region, Russian). *Ore Geol. Rev.* **2001**, *17*, 215–232. [[CrossRef](#)]
25. Chen, Y.J.; Chen, H.Y.; Zaw, K. Geodynamic settings and Tectonic Model of Skarn Gold Deposits in China: An Overview. *Geol. Rev.* **2007**, *31*, 139–169. [[CrossRef](#)]
26. Zhang, Y.; Sun, J.G.; Xing, S.W.; Zhao, K.Q.; Ma, Y.B. Geochronology and metallogenesis of porphyry Mo deposits in east-central Jilin province, China: Constraints from molybdenite Re–Os isotope systematics. *Ore Geol. Rev.* **2015**, *71*, 363–372. [[CrossRef](#)]
27. Qiu, K.F.; Yu, H.C.; Wu, M.Q.; Geng, J.Z.; Ge, X.K.; Gou, Z.; Taylor, R.D. Discrete Zr and REE mineralization of the Baerzhe rare-metal deposit, China. *Am. Mineral.* **2019**. [[CrossRef](#)]
28. Li, W.B.; Huang, Z.L.; Zhang, G. Sources of the ore metals of the Huize ore field in Yunnan province: Constraints from Pb, S, C, H, O and Sr isotope geochemistry. *Acta Petrol. Sin.* **2006**, *22*, 2561–2580. (In Chinese with English Abstract)
29. Yin, A.; Nie, S. *A Phanerozoic Palinspastic Reconstruction of China and Its Neighboring Regions*; Cambridge University Press: Cambridge, UK, 1996.
30. Yang, X.M. Using the Rittmann Serial Index to define the alkalinity of igneous rocks. *Neues Jahrb. Mineral. Abh.* **2007**, *184*, 95–109.
31. Sun, J.G.; Zhang, Y.; Xing, S.W.; Zhao, K.Q.; Zhang, Z.J.; Bai, L.A.; Ma, Y.B.; Liu, Y.S. Genetic types, ore-forming age and geodynamic setting of endogenic molybdenum deposits in the eastern edge of Xing-Meng orogenic belt. *Acta Petrol. Sin.* **2012**, *28*, 1317–1332. (In Chinese with English Abstract)
32. Xiao, W.J.; Windley, B.F.; Hao, J. Accretion Leading to Collision and the product Solonker Suture, Inner Mongolia, China: Termination of the Central Asian Orogenic Belt. *Tectonics* **2003**, *22*, 1069. [[CrossRef](#)]

33. Ge, W.C.; Wu, F.Y.; Zhou, C.Y.; Zhang, J.H. Metallogenic epoch and geodynamic significance of porphyry Cu–Mo deposits in the eastern part of Xing-Meng Orogenic Belt. *Chin. Sci. Bull.* **2007**, *52*, 2407–2417. (In Chinese) [[CrossRef](#)]
34. Taylor, H.P. The application of oxygen and hydrogen isotope studies to problems of hydrothermal alteration and ore deposition. *Econ. Geol.* **1974**, *69*, 843–883. [[CrossRef](#)]
35. White, W.M. *Geochemistry*; John Wiley and Sons Ltd.: Hoboken, NJ, USA, 2013; pp. 406–409.
36. Zartman, R.E.; Doe, B.R. Plumbotectonics the model. *Tectonophysics* **1981**, *75*, 135–162. [[CrossRef](#)]
37. Wu, M.Q.; Tian, B.F.; Zhang, D.H.; Xu, G.Z.; Xu, W.X.; Qiu, K.F. Zircon of the No. 782 deposit from the Great Xing’an Range in NE China: Implications for Nb-REE-Zr mineralization during magmatic-hydrothermal evolution. *Ore Geol. Rev.* **2018**, *102*, 284–299. [[CrossRef](#)]
38. Chen, Y.J.; Chen, H.Y.; Liu, Y.L. Progress and Records in the Study of Endogenetic Mineralization During Collisional Orogenesis. *Chin. Sci. Bull.* **2000**, *45*, 1–10. (In Chinese with English Abstract) [[CrossRef](#)]
39. Li, N.; Chen, Y.J.; Ulrich, T. Fluid Inclusion Study of the Wunugetu Cu–Mo Deposit, Inner Mongolia, China. *Miner. Depos.* **2012**. [[CrossRef](#)]
40. Li, L.X.; Song, Q.H.; Wang, D.H.; Wang, C.H.; Qu, W.J.; Wang, Z.G.; Bi, S.Y.; Yu, C. Re–Os isotopic dating of molybdenite from the Fu’anbu Molybdenum deposit of Jilin province and discussion on its metallogenesis. *Rock Miner. Anal.* **2009**, *28*, 283–287. (In Chinese with English Abstract)
41. Shao, J.B.; Chen, D.Y.; Pan, Y.D.; Wang, H.T. Re–Os isotopic dating of molybdenites from Jidetun and Shimadong large molybdenum deposits in centro-eastern Jilin and its geological significance. *Glob. Geol.* **2016**, *35*, 717–728. (In Chinese with English Abstract)
42. Wang, C.H.; Song, Q.H.; Wang, D.H.; Li, L.X.; Yu, C.; Wang, Z.G.; Qu, W.J.; Du, A.D.; Ying, L.J. Re–Os isotopic dating of molybdenite from the Daheishan molybdenum deposit of Jilin province and its geological significance. *Rock Miner. Anal.* **2009**, *28*, 269–273. (In Chinese with English Abstract)
43. Wu, F.Y.; Jahn, B.M.; Wilde, S.A.; Sun, D.Y. Phanerozoic continental crustal growth: U–Pb and Sr–Nd isotopic evidence from the granites in northeastern China. *Tectonophysics* **2000**, *328*, 89–113. [[CrossRef](#)]
44. Qiu, K.F.; Marsh, E.; Yu, H.C.; Pfaff, K.; Gulbransen, C.; Gou, Z.Y.; Li, N. Fluid and metal sources of the Wenquan porphyry molybdenum deposit, Western Qinling, NW China. *Ore Geol. Rev.* **2017**, *86*, 459–473. [[CrossRef](#)]
45. Qiu, K.F.; Song, K.R.; Song, Y.H. Magmatic-hydrothermal fluid evolution of the Wenquan porphyry molybdenum deposit in the north margin of the Western Qinling, China. *Acta Petrol. Sin.* **2015**, *31*, 3391–3404. (In Chinese with English Abstract)
46. Ren, Y.S.; Ju, N.; Zhao, H.L.; Wang, H.; Hou, K.J.; Liu, S. Geochronology and Geochemistry of Metallogenic Porphyry Bodies from Nongping Au–Cu Deposit in Eastern Yanbian, NE China: Implications for Depositional Environment. *Acta Geol. Sin.* **2012**, *86*, 619–629.
47. Wu, F.Y.; Liu, X.C.; Ji, W.Q.; Wang, J.M.; Yang, L. Highly fractionated granites: Recognition and research. *Sci. China Earth Sci.* **2017**, *60*, 1201–1219. (In Chinese with English Abstract) [[CrossRef](#)]

